Characterizing seabed sediments using multi-spectral backscatter data in the North Sea

Qian Bai*, Sebastiaan Mestdagh*, Mirjam Snellen* and AliReza Amiri-Simkooei†
*Faculty of Aerospace Engineering
Delft University of Technology, Delft, The Netherlands
Email: q.bai@tudelft.nl
†Faculty of Civil Engineering and Geosciences
Delft University of Technology, Delft, The Netherlands

OCEANS 2023 - Limerick | 979-8-3503-3226-1/23/$31.00 ©2023 IEEE | DOI: 10.1109/OCEANSLimerick52467.2023.10244650

***Abstract*—Acoustic classification using single-beam and multi-beam echosounders has been widely applied in characterizing seabed sediments. Although previous studies have shown a better discrimination of fine and coarse sediments using multi-spectral echosounder data, analysis regarding comprehensive seabed sediment properties is still needed. In this study, we used single-beam data of 24 kHz, as well as multi-beam data of 90 and 300 kHz to investigate the benefits of multi-spectral backscatter data in describing sediment properties including median grain size; weight percentages of gravel, sand, and mud; volume percentages of stones, shell fragments, and living bivalves; as well as density of acoustically hard animals (molluscs and the tube-building worm *Lanice conchilega*). We classified data of each frequency in an unsupervised manner, using K-means clustering for the single-beam echo time series and Bayesian classification for the multi-beam backscatter. Compared with the top-layer sediment properties, we found classification of 90 and 300 kHz consistent with variations of median grain size and *L. conchilega* density, whereas classification of 24 kHz can also be related to the percentages of shell fragments and stones. In addition, one acoustic class of 24 kHz might indicate a higher gravel content in the subsurface of the study area. Although quantitative relationships between backscatter and sediment properties are still difficult to achieve given a limited number of samples, using multi-spectral backscatter data is a potential approach to characterize seabed sediments from various perspectives.**

***Index Terms*—seabed sediment, single-beam echosounder, multi-beam echosounder, backscatter, multi-spectral, acoustic classification, North Sea**

I. Introduction

Seabed sediment information is essential for various marine applications, including habitat conservation and planning of offshore constructions [1, 2]. Compared to bottom sampling, which provides sparsely distributed seabed information, acoustic remote sensing techniques measure broad-scale sediment properties more efficiently and cost-effectively. Acoustic backscatter, the intensity of an acoustic signal scattered from the seabed, is affected by sediment properties such as interface roughness and volume heterogeneity [3], making it a useful tool for seabed mapping.

In the past decades, two acoustic remote sensing techniques have been widely used to characterize the seabed: single-beam echosounders (SBES) and multi-beam echosounders (MBES). SBES acquire an acoustic signal directly below the echosounder from each ping, whereas MBES form hundreds of beams in a swath perpendicular to the sailing direction by emitting one ping, achieving a much larger coverage of the seabed. Nevertheless, SBES are still extensively used since they are less expensive and require simpler operations [4]. With SBES or MBES data, seabed sediments can be characterized by linking properties like mean grain size to acoustic backscatter or its derivatives, such as echo shape and image texture features. Common methods include model-based and empirical seabed classification.

In model-based methods, physical models based on laboratory measurements are used [5]. The sediment type can be determined through model inversion given the backscatter strength from a certain frequency and incident angle [6, 7]. Although bottom samples are not needed in these methods, absolute backscatter calibration of sonar characteristics is. In addition, physical models have not considered biological communities, making it difficult to apply model-based methods in habitat mapping. Empirical methods, on the other hand, require a few samples from the seabed to establish the relationship between backscatter and sediment properties, either by supervised [8, 9] or unsupervised classification [10, 11]. However, absolute or relative calibration can be avoided as long as the relative variation of backscatter measurements can represent the changes in sediments [12], making data processing much easier.

Although previous research has demonstrated the success of classifying seabed sediments using empirical methods, these studies have usually been restricted to one acoustic frequency. When the sediment grain size is smaller than the acoustic wavelength, unambiguous classification of sediment types can be achieved. Otherwise, fine and coarse sediment might result in similar backscatter strength [13]. Thus, single-frequency analysis might not be able to discriminate coarse sediments like shell fragments [14]. With the recent development of multi-spectral echosounders, the benefit of combining multiple frequencies in sediment characterization is being investigated. Runya et al. [15] found a stronger correlation between the mean grain size and backscatter strength with MBES data of 30 kHz than 95 and 300 kHz in an area consisting of sediments from sand to gravel. Brown et al. [16] and Menandro et al. [17] showed the advantage of lower frequencies in distinguishing fine sediments due to a deeper penetration. Gaida et al. [12]

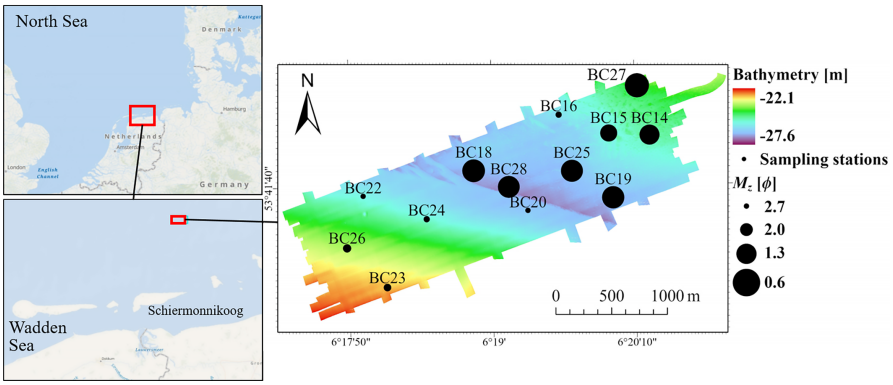

Fig. 1. Study area north of the Wadden Sea island Schiermonnikoog, showing bathymetry, sampling stations, and median grain size (M_z) from the top sediment layer.

also pointed out that classification of lower frequencies might indicate rough materials in the shallow subsurface below the muddy sediment. They further developed a multi-spectral Bayesian classification method for MBES data. By combining 100 and 400 kHz, they achieved a more complete view of both the seabed surface and subsurface sediment than the single-frequency results.

However, research on multi-spectral classification of other sediment properties, such as the amount of shell fragments and the occurrence of marine benthos, is lacking. The goal of this study is to characterize the seabed sediment more accurately, by accounting for these elements using multi-spectral backscatter data. To accomplish this, we analyze a MBES dataset consisting of backscatter data at 90 and 300 kHz using an unsupervised Bayesian classification method [11]. To further enlarge the frequency range, we also use SBES data of 24 kHz. We extract the echo shape features and assign them to several acoustic classes using K-means clustering. All classification results are then compared with bottom samples to investigate the relationship between acoustic classification of different frequencies and various sediment properties, such as median grain size, presence of shell fragments, and abundance of benthos. Additionally, considering the possible penetration of 24 kHz into the sediment, interpreting the classification results requires not only surface samples, but the subsurface properties need to be taken into account [18]. Thus, we also use samples from a deeper sediment layer to investigate the possibility of describing subsurface properties with lower frequencies. Through the comprehensive analysis, we show the potential of using multi-spectral backscatter for seabed sediment characterization, which is of great importance for managing marine habitats.

II. Materials and Methods

A. Acoustic Data Acquisition

We obtained the acoustic data north of the Wadden Sea island Schiermonnikoog in the North Sea in August 2021 (Fig. 1). The area shows gradual bathymetric changes in the shallower western region, followed by a steep drop and a more heterogeneous region in the east. The water depth varies from 22.1 to 27.6 m. We collected the MBES data, including the two frequencies 90 and 300 kHz, using a multi-spectral multi-beam system R2Sonic 2026 (R2Sonic, Austin, TX, USA). The beam widths are 2.3° and 0.7° for 90 and 300 kHz, respectively. We adopted a swath coverage of 130°. In addition, we collected SBES data of 24 kHz using a single-beam system Kongsberg EA440 (Kongsberg Gruppen, Kongsberg, Norway), with a beam width of 20°.

B. SBES Data Processing

The original SBES data were stored as RAW files. We converted them into the EA400 format using the Kongsberg software EA440 and extracted the echo time series of each ping using a MATLAB toolbox *readEKRaw*. Before feature extraction, we corrected the time series for the sonar settings and transmission loss of acoustic signals [10]:

$$I = I_r - 10\log P_t + 40\log R + 2\alpha R - 2G - 10\log R, \quad (1)$$

where I is the received intensity (dB), I_r the corrected intensity (dB), P_t the transmitted power (W), R the range from the transducer to the detected sea bottom (m), α the absorption coefficient (dB/m), and G the transmitter or receiver gain (dB). The last term $10\log R$ accounts for the signal footprint effect, by assuming that the footprint size is proportional to the depth below the transducer. Since the echosounder was installed along the vertical axis, we treated R the same as depth. In addition, to remove the impact of depth on the echo shape, we scaled the time series from each ping according to

$$t_n = \frac{R_{ref}}{R} t, \quad (2)$$

where t is the received time (s), t_n the normalized time (s), and R_{ref} the reference depth (m). To validate the effectiveness of depth correction, we also generated features from simulated SBES echo time series (see section III-A). The simulation was based on the APL model [5], with median grain size, water depth, and sonar parameters (e.g., frequency, pulse length, and transducer diameter) as input.

We followed the feature extraction process proposed by van Walree et al. [19] and calculated three features from the

corrected time series (t_n,I) of each ping: total energy, time spread, and skewness. Whereas total energy is the integrated intensity of the time series, time spread measures how fast the echo intensity drops after reaching the maximum. Skewness indicates asymmetry, which can be affected by, for example, an elongated tail and a possible second peak for deeper layers. All three features can be affected by the seabed sediment hardness, roughness, the amount of volume scattering, and the presence of hard materials in the subsurface. To avoid including noise from the water column, we calculated these features on the time series from the maximum intensity until 0.045 s. We selected the truncation time based on sufficient visual inspections.

To alleviate random fluctuations of the backscattering process, we averaged these features over 30 consecutive pings. We also conducted a principal component analysis (PCA) to reduce the number of features and remove possible statistical correlations among the features. Afterwards, we clustered the first two principal components (PCs) using the K-means clustering algorithm [20], with the optimal number of classes selected using silhouette coefficients [21].

C. MBES Data Processing

We first cleaned the MBES data for bathymetric outliers using the QPS software Qimera. We then divided the data into different frequencies and converted them to the generic sensor format (GSF). With the received echo level extracted from the GSF files, we applied backscatter correction to obtain an averaged backscatter strength (in dB per m^2 at 1 m) per beam, which can represent the actual seabed properties. We removed the impact of sonar characteristics, including the source level, time varying gain, and beam pattern effect. The two-way transmission loss and seawater absorption were also accounted for.

In this study, we avoided the backscatter angular normalization used in many empirical classification methods [22–24], because such normalization might induce unexplained uncertainties [25]. Instead, we considered individual beams using Bayesian classification developed by Simons and Snellen [11]. Since the backscatter strength per beam is the result of averaging over many independent scatter pixels (the ensonified area of a transmitted pulse), it can be assumed to fulfill the central limit theorem, and hence to follow a normal distribution. The histogram of the backscatter strength from a single incident angle and frequency can then be modeled as a summation of m Gaussian distributions, assuming m sediment types in the surveyed area. The optimal m is determined by fitting an increasing number of Gaussians to satisfy the χ^2 statistical test.

To ensure the robustness of classification, we chose several reference incident angles between 40° and 60° based on their χ^2 test results and consistency in the fitted Gaussian distributions. The average percentage distribution of the boundaries between fitted Gaussians at these angles defines the expected presence of classes, which was then applied to other incident angles. In addition, we excluded incident angles smaller than 20°, since there are too few scatter pixels, and hence the central limit theorem cannot be satisfied.

D. Ground Truth Samples

We selected 13 sampling stations for both sediment and macrofauna analysis. We took three boxcore samples at each location, with two replicates for macrofauna analysis and a third sample for sediment. The depth of each replicate is between 20 and 25 cm. The macrofauna replicates were sieved on board through a 1 mm mesh to extract the fauna. Fauna were stored in a 4% formalin solution before the laboratory analysis. Acoustically hard animals, such as molluscs and the tube-building sand mason worm *Lanice conchilega*, were identified to species level, while other animals only to class or order level. All animals were counted to obtain their density (individuals per m^2). The sediment sample was analyzed to determine properties such as median grain size (d_{50} in mm) and weight percentage of gravel, sand, and mud. The median grain size is also commonly expressed in ϕ units as $M_z = -\log_2 d_{50}$. Additionally, volume percentages of shell fragments ($>$ 10 mm), living bivalves, and stones ($>$ 4 mm) were determined.

We adopted a two-layer strategy for the sample analysis. The macrofauna replicates were analyzed separately for depths smaller and larger than 10 cm. For the sediment sample, we treated the top 5 cm as the first layer. The second layer ranged from 5 to 20 cm, or to a visible change in the subsurface sediment. For simplicity, we will refer to the two layers in all samples as the top layer and the deeper layer. To explicitly investigate differences between the two layers, we applied PCA to all sample properties for each layer. We then compared the primary feature, the first PC, of both layers.

III. Results and Discussion

A. SBES Feature Extraction

With the range of M_z in our study area, we calculated the expected total energy, time spread, and skewness from the simulated echo time series (Fig. 2). We also used varying water

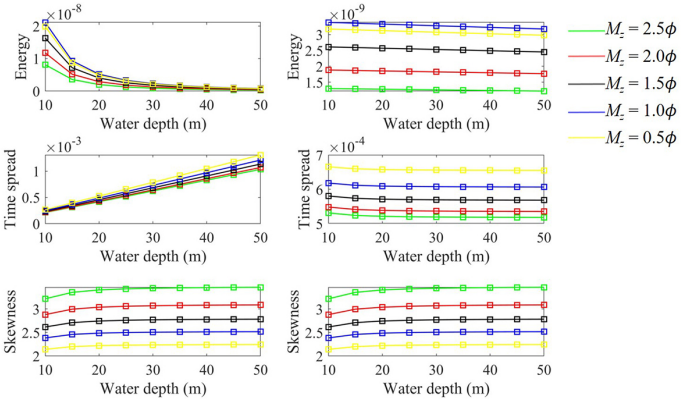

Fig. 2. Simulated total energy, time spread, and skewness using the APL model for different water depths (Left) before and (Right) after depth correction.

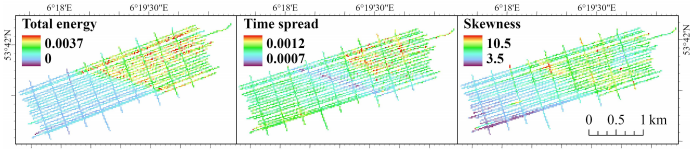

Fig. 3. Total energy, time spread, and skewness of the study area.

depth (from 10 to 50 m) to show the influence of depth on these features. Total energy and time spread were originally susceptible to water depth, but our depth correction could remove this dependence, making both features discriminative for different sediment types and independent of depth (see the two upper right subplots in Fig. 2). On the other hand, skewness was not affected by water depth. It is common in some studies to derive the volume backscatter strength from the SBES data by accounting for the ensonified water volume. This can be suitable for detecting fish and crabs [26, 27]. Since we focused on the sediment properties, we considered more the acoustic backscatter from the seabed. The ensonified footprint geometry can be calculated rigorously when the sonar characteristics are clearly known [28]. Otherwise, we can use the depth correction described in this paper to achieve effective comparisons among regions.

We applied all corrections described in section II-B to the SBES measurements. Features from the corrected echo time series showed regional patterns in the study area (Fig. 3). While total energy indicated a relatively homogenous seabed in the west, time spread and skewness showed gradual variations. Near the steep drop in the middle of the area, total energy and skewness had higher values than in the west, which might be due to coarser sediment. In contrast, time spread was the lowest here, possibly indicating less volume scattering or smaller seabed roughness. For the eastern deeper seabed, all three features showed heterogeneous patterns, with different areas highlighted with the highest values.

We also compared these three features calculated from our measurements near all sampling stations and model simulations generated with similar M_z as the samples (Fig. 4). Although their values were not comparable without absolute sonar calibration, the trend of total energy with M_z was generally consistent for the measurements and the model. Total energy increased with median grain size at first due to the enlarging acoustic impedance. However, for even coarser sediments, total energy became lower, possibly because more acoustic signals were scattered with a fixed beam width of SBES [7]. The trend of measured time spread and skewness deviated from the model to some extent. Since model simulations only had M_z as input, we might need to consider more seabed properties, such as presence of benthos and subsurface characteristics, when interpreting features from our measurements.

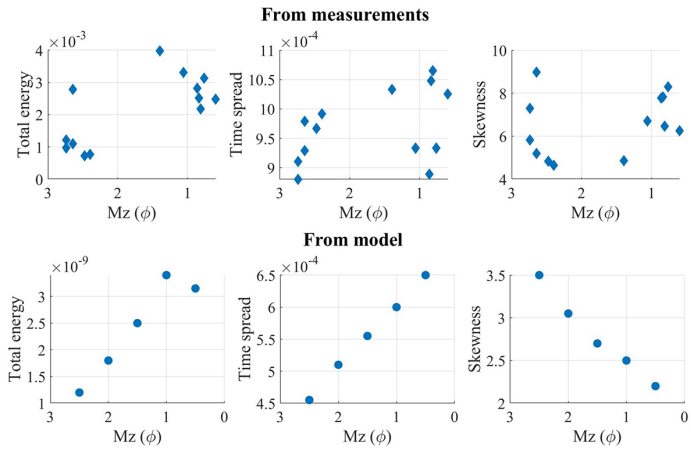

Fig. 4. Comparison between SBES features from the measurements and model calculations with a depth of 25 m.

B. Acoustic Seabed Classification

Based on the silhouette coefficients and the χ^2 statistical test, we selected 3, 4, and 4 classes for data of 24 kHz (SBES), 90 kHz (MBES), and 300 kHz (MBES) in this study. Acoustic classification of both SBES and MBES data indicated a generally homogenous sediment of the western shallower seabed (Fig. 5). In the east, SBES data were clearly divided into two classes, in which class 3 corresponded especially to regions with the highest time spread. With a much higher point density and thus a better spatial resolution than the SBES data, MBES classification revealed more detailed variations on the eastern seabed. In general, class 3 and 4 indicated similar spatial distributions for 90 and 300 kHz. Class 3 covered slightly different areas between 90 kHz and 300 kHz.

Differences in acoustic classification for data with various frequencies might indicate their different responses with the same sediment or different penetration abilities. For SBES data of 24 kHz, classification was possibly affected by the subsurface properties given sufficient penetration. On the other hand, we involved different incident angles for SBES and MBES classification. While SBES acquired data from the nadir, our MBES data covered a larger swath reaching 65° on both the port and starboard sides. Combining these data from different frequencies might help us achieve more complete interpretations of the study area, but brought some difficulty in independently analyzing the influence of acoustic frequencies.

C. Comparison between Acoustic Classes and Top-layer Ground Truth

To investigate if acoustic classification could represent the actual variation of sediments, we compared acoustic classes

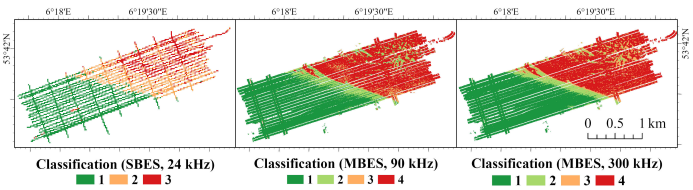

Fig. 5. Acoustic classification of SBES and MBES data.

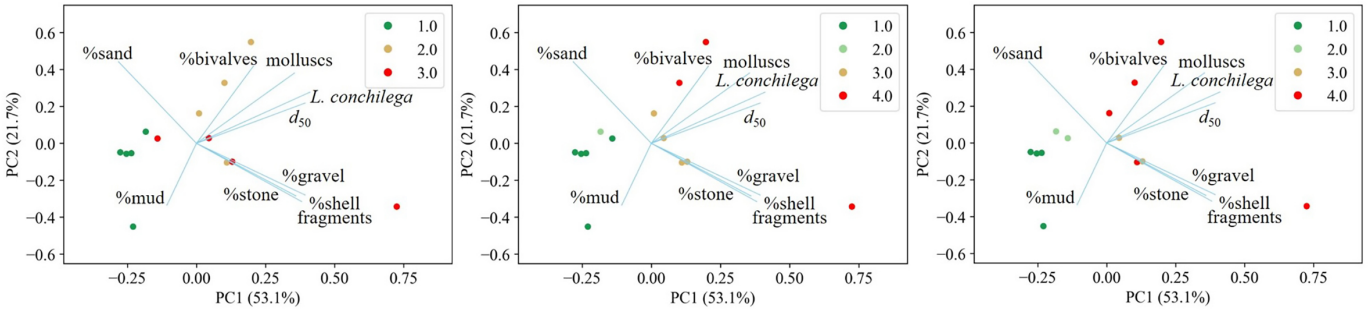

Fig. 6. Biplot of top-layer sample properties. Each point represents a sampling station, with point colors indicating acoustic classes from (Left) SBES echo time series at 24 kHz, (Middle) MBES backscatter at 90 kHz, and (Right) MBES backscatter at 300 kHz. We use d_{50} instead of M_z for PCA here to show the positive impact of median grain size on backscatter more conveniently.

with PCA results of the sample properties. We first constrained the comparison to the top sediment layer. Even with a deeper penetration into the sediment, surface roughness and volume heterogeneity of the top layer can still affect the acoustic backscatter. With the sample property vectors projected on the span of the first and second PC, we saw the primary variation in sediments contributed by d_{50}, *L. conchilega* density, and gravel content (Fig. 6). In addition, percentages of sand, stone, gravel, and shell fragments were highly correlated. Mollusc density, *L. conchilega* density, and d_{50} also showed positive correlations.

We also constructed PCA biplots of the first and second PC, with acoustic classification of the samples indicated by colors (Fig. 6). Class 1 of 24, 90, and 300 kHz were generally consistent with an aggregation of samples with fine sediments and less benthos. For 90 and 300 kHz, the gradient of acoustic classes was especially along with changes of d_{50} and *L. conchilega* density, showing the correspondence between MBES classification and the primary sediment properties. Additionally, difference between 90 and 300 kHz was relatively small, considering that our study area only included fine to coarse sand. As an important benthic species in the North Sea, *L. conchilega* builds tubes with sand and shell fragments, which can protrude out of the sediment for several centimeters, thereby increasing the local seabed roughness [29–31].

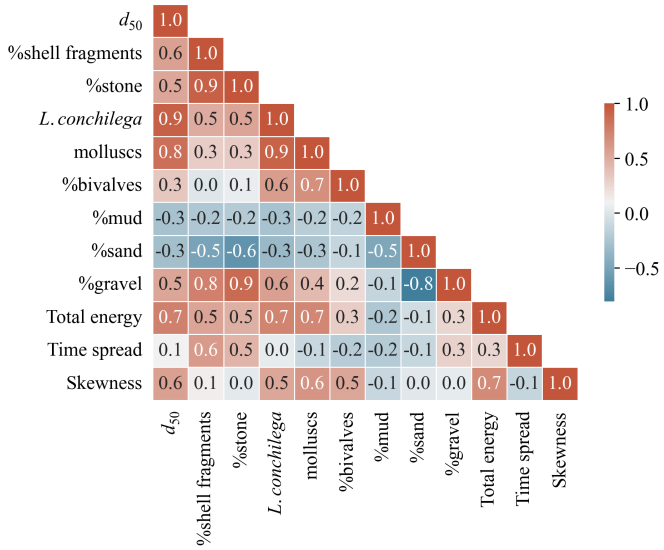

Fig. 7. Pearson correlation coefficients between SBES features and top-layer sediment properties.

In contrast, classification of 24 kHz did not vary with d_{50} only. For SBES features, although total energy was highly correlated with d_{50} and *L. conchilega* density, there was also moderate correlation with shell fragments (Fig. 7). This latter correlation, albeit higher, was also found for time spread. Considering the wavelengths of 24, 90, and 300 kHz, which are 63, 17, and 5 mm, it is possible that acoustic signals of 24 kHz are more sensitive to variations in coarse materials such as shell fragments ($>$ 10 mm) and stones ($>$ 4 mm). In addition, modeled time spread barely showed the impact of more volume scattering in finer sediments for 24 kHz (Fig. 4), probably indicating that SBES features were mainly affected by the seabed roughness that can be altered by the amount of shell fragments and stones.

Considering a higher spatial resolution of MBES data, classification for 90 and 300 kHz might be more consistent with the small-scale information represented by boxcore samples [32]. Compared to MBES, although our SBES data had limited seabed coverage, we could still achieve a general distribution of the sediment properties.

D. Indication on Subsurface Properties

Different classification between 24 kHz and the other two higher frequencies might also be attributed to acoustic backscatter of 24 kHz below the subsurface. To investigate the possible influence of subsurface properties, we compared the first PC from the top and deeper sediment layer (Fig. 8). Since *L. conchilega* tubes have a vertically elongated shape, which can be longer than 10 cm, and very few of them were found in the deeper layer, we assumed they contributed similarly to both sediment layers and excluded them from this analysis. Considering other sample properties, both layers of our study area were similar to each other in general. Difference between them could be found in samples BC16, BC25, and BC27. Although these samples had little difference in d_{50} between

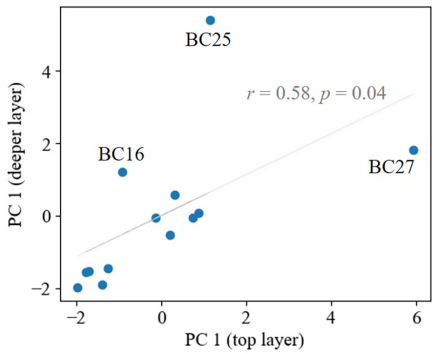

Fig. 8. The first PC from top-layer properties versus the first PC from deeper-layer properties.

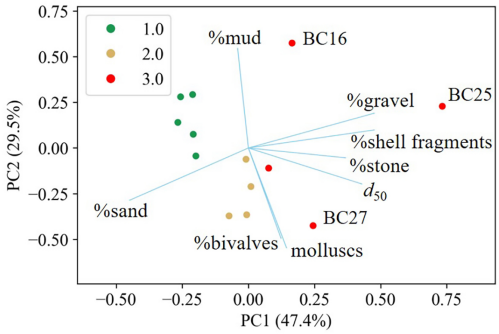

Fig. 9. Biplot of deeper-layer properties, with point color indicating the SBES classification of 24 kHz.

the top and deeper layer, BC16 and BC25 showed much higher gravel content in the deeper layer, which was also consistent with areas showing high values of the SBES feature time spread.

In addition, we saw a clear gradient of acoustic classes of 24 kHz along the first PC from the deeper-layer sample properties, to which the percentages of gravel, shell fragments, stones, and d_{50} mostly contributed (Fig. 9). Thus, class 3 of 24 kHz might indicate a subsurface layer with coarse materials in the eastern region of our study area. To confirm this, the penetration depth of acoustic signals in such a sandy environment needs to be investigated more thoroughly.

IV. Conclusion

Acoustic remote sensing is an important tool for characterizing seabed sediments. In this study, we used SBES and MBES data of three frequencies, 24, 90, and 300 kHz, to investigate the benefits of multi-spectral backscatter data in describing comprehensive sediment properties in an area near the western Wadden Sea islands in the North Sea.

For the SBES echo time series of 24 kHz, we applied corrections to remove the impact of water depth and some sonar characteristics. The resulting SBES features (total energy, time spread, and skewness) were validated to be distinguishable for different sediment types based on the APL model simulations. We further classified these features using K-means clustering. We also classified MBES backscatter data of 90 and 300 kHz in an unsupervised way by Bayesian classification, which accounts for the statistical variations of the backscatter strength within a beam. To investigate the impact of various sediment properties, we considered median grain size; weight percentages of gravel, sand, and mud; volume percentages of stones, shell fragments, and living bivalves; as well as density of acoustically hard animals *L. conchilega* and molluscs from 13 boxcore samples. These sample properties were also analyzed for the top and deeper sediment layer separately to achieve a better understanding of the study area.

By comparing acoustic classification results with the top-layer sample properties, we found MBES classification of 90 and 300 kHz consistent with the variation of median grain size and *L. conchilega* density, but the difference between 90 and 300 kHz was small. In contrast, SBES classification of 24 kHz could also be affected by the presence of shell fragments and stones. Additionally, we did not see apparent layering of sediments in our study area by comparing the PCA results between top- and deeper-layer sample properties. The main difference might be a higher gravel content of the subsurface sediment in the eastern region. Considering the clear gradient of acoustic classification of 24 kHz with variations in the deeper-layer properties, it is possible that acoustic signals of 24 kHz reached the subsurface or were reflected by suspended coarse materials in the sediment, but further study of the penetration depth is needed to support this finding.

Limited by the data itself, it is relatively difficult to solely assess the impact of acoustic frequencies without involving different incident angles and spatial resolutions. Nevertheless, in this study, acoustic classification of SBES and MBES data for various frequencies can represent different sediment properties, making it a potential approach to use multi-spectral backscatter data for better seabed characterization. With a good selection of the frequency range, the multi-spectral strategy is valuable for monitoring marine habitats from different perspectives in the long term.

Acknowledgment

The research is part of the NWO-funded project 18698 "Multi-spectral Multi-beam Imaging for Mapping the Occurrence of Marine Benthos". We express our gratitude to Rijkswaterstaat for their support in the survey planning and measurements on board. Special thanks to Helga van der Jagt, Paula Neijenhuis and Rebecca Bakker (Bureau Waardenburg) for their help on board and their colleagues for sample analyses. QPS, R2Sonic, Van Oord, Boskalis and Deltares are also acknowleged for providing the software licenses, sonar equipment and the technical support.

References

[1] C. J. Brown, S. J. Smith, P. Lawton, and J. T. Anderson, "Benthic habitat mapping: A review of progress towards improved understanding of the spatial ecology of the seafloor using acoustic techniques," *Estuarine, Coastal and Shelf Science*, vol. 92, pp. 502–520, Mar. 2011.

[2] G. Lamarche and X. Lurton, "Recommendations for improved and coherent acquisition and processing of backscatter data from seafloor-mapping sonars," *Marine Geophysical Research*, vol. 39, p. 5–22, 2018.

[3] X. Lurton, *An introduction to underwater acoustics*. Springer Berlin, Heidelberg, 2002.

[4] M. M. L. Figueroa, M. J. G. Parsons, B. J. Saunders, B. Radford, C. Salgado-Kent, and I. M. Parnum, "The use of singlebeam echo-sounder depth data to produce demersal fish distribution models that are comparable to models produced using multibeam echo-sounder depth," *Ecology and Evolution*, vol. 11, pp. 17 873–17 884, Dec. 2021.

[5] Applied Physics Laboratory, University of Washington, "APL-UW high-frequency ocean environmental acoustic models handbook," Applied Physics Laboratory, University of Washington, Seattle, WA, USA, Tech. Rep. APL-UW TR9407, Oct. 1994.

[6] L. Fonseca and L. Mayer, "Remote estimation of surficial seafloor properties through the application angular range analysis to multibeam sonar data," *Marine Geophysical Researches*, vol. 28, p. 119–126, Jun. 2007.

[7] M. Snellen, K. Siemes, and D. G. Simons, "Model-based sediment classification using single-beam echosounder signals," *The Journal of the Acoustical Society of America*, vol. 129, pp. 2878–2888, May 2011.

[8] D. Ierodiaconou, J. Monk, A. Rattray, L. Laurenson, and V. Versace, "Comparison of automated classification techniques for predicting benthic biological communities using hydroacoustics and video observations," *Continental Shelf Research*, vol. 31, pp. S28–S38, Feb. 2011.

[9] D. Stephens and M. Diesing, "A comparison of supervised classification methods for the prediction of substrate type using multibeam acoustic and legacy grain-size data," *PLoS One*, vol. 9, p. e93950, Apr. 2014.

[10] A. Amiri-Simkooei, M. Snellen, and D. G. Simons, "Principal component analysis of single-beam echo-sounder signal features for seafloor classification," *IEEE Journal of Oceanic Engineering*, vol. 36, pp. 259–272, Apr. 2011.

[11] D. G. Simons and M. Snellen, "A Bayesian approach to seafloor classification using multi-beam echo-sounder backscatter data," *Applied Acoustics*, vol. 70, pp. 1258–1268, Oct. 2009.

[12] T. C. Gaida, T. A. T. Ali, M. Snellen, A. Amiri-Simkooei, T. A. G. P. V. Dijk, and D. G. Simons, "A multispectral Bayesian classification method for increased acoustic discrimination of seabed sediments using multi-frequency multibeam backscatter data," *Geosciences*, vol. 8, p. 455, Dec. 2018.

[13] D. Eleftherakis, M. Snellen, A. Amiri-Simkooei, and D. G. Simons, "Observations regarding coarse sediment classification based on multi-beam echo-sounder's backscatter strength and depth residuals in dutch rivers," *The Journal of the Acoustical Society of America*, vol. 135, pp. 3305–3315, Jun. 2014.

[14] J. E. H. Clarke, "Multispectral acoustic backscatter from multibeam, improved classification potential," in *Proceedings of the United States Hydrographic Conference*, San Diego, CA, USA, Mar. 2015, pp. 16–19.

[15] R. M. Runya, C. McGonigle, R. Quinn, J. Howe, J. Collier, C. Fox, J. Dooley, R. O'Loughlin, J. Calvert, L. Scott, C. Abernethy, and W. Evans, "Examining the links between multi-frequency multibeam backscatter data and sediment grain size," *Remote Sensing*, vol. 13, p. 1539, Apr. 2021.

[16] C. J. Brown, J. Beaudoin, M. Brissette, and V. Gazzola, "Multispectral multibeam echo sounder backscatter as a tool for improved seafloor characterization," *Geosciences*, vol. 9, p. 126, Mar. 2019.

[17] P. S. Menandro, A. C. Bastos, B. Misiuk, and C. J. Brown, "Applying a multi-method framework to analyze the multispectral acoustic response of the seafloor," *Frontiers in Remote Sensing*, vol. 3, Mar. 2022.

[18] B. Misiuk and C. J. Brown, "Multiple imputation of multibeam angular response data for high resolution full coverage seabed mapping," *Marine Geophysical Research*, vol. 43, p. 7, Mar. 2022.

[19] P. A. van Walree, J. Tęgowski, C. Laban, and D. G. Simons, "Acoustic seafloor discrimination with echo shape parameters: A comparison with the ground truth," *Continental Shelf Research*, vol. 25, pp. 2273–2293, Nov. 2005.

[20] G. A. F. Seber, *Multivariate observations*. John Wiley & Sons, 2009.

[21] P. J. Rousseeuw, "Silhouettes: A graphical aid to the interpretation and validation of cluster analysis," *Journal of Computational and Applied Mathematics*, vol. 20, pp. 53–65, Nov. 1987.

[22] X. Cui, H. Liu, M. Fan, B. Ai, D. Ma, and F. Yang, "Seafloor habitat mapping using multibeam bathymetric and backscatter intensity multi-features svm classification framework," *Applied Acoustics*, vol. 174, p. 107728, Mar. 2021.

[23] M. Diesing, S. L. Green, D. Stephens, R. M. Lark, H. A. Stewart, and D. Dove, "Mapping seabed sediments: Comparison of manual, geostatistical, object-based image analysis and machine learning approaches," *Continental Shelf Research*, vol. 84, pp. 107–119, Aug. 2014.

[24] L. Janowski, K. Trzcinska, J. Tegowski, A. Kruss, M. Rucinska-Zjadacz, and P. Pocwiardowski, "Nearshore benthic habitat mapping based on multi-frequency, multibeam echosounder data using a combined object-based approach: A case study from the rowy site in the southern baltic sea," *Remote Sensing*, vol. 10, p. 1983, Dec. 2018.

[25] L. Hamilton and I. Parnum, "Acoustic seabed segmentation from direct statistical clustering of entire multibeam sonar backscatter curves," *Continental Shelf Research*, vol. 31, pp. 138–148, Feb. 2011.

[26] J. M. Jech, G. L. Lawson, and A. C. Lavery, "Wideband (15-260 kHz) acoustic volume backscattering spectra of Northern krill (*Meganyctiphanes norvegica*) and butterfish (*Peprilus triacanthus*)," *ICES Journal of Marine Science*, vol. 74, p. 2249–2261, Sep./Oct. 2017.

[27] R. A. McConnaughey and S. E. Syrjala, "Statistical relationships between the distributions of groundfish and crabs in the eastern bering sea and processed returns from a single-beam echosounder," *ICES Journal of Marine Science*, vol. 66, p. 1425–1432, Jul. 2009.

[28] D. Eleftherakis, L. Berger, N. L. Bouffant, A. Pacault, J. M. Augustin, and X. Lurton, "Backscatter calibration of high-frequency multibeam echosounder using a reference single-beam system, on natural seafloor," *Marine Geophysical Research*, vol. 39, p. 55–73, Feb. 2018.

[29] S. Degraer, G. Moerkerke, M. Rabaut, G. V. Hoey, I. D. Four, M. Vincx, J. P. Henriet, and V. V. Lancker, "Very-high resolution side-scan sonar mapping of biogenic reefs of the tube-worm *Lanice conchilega*," *Remote Sensing of Environment*, vol. 112, pp. 3323–3328, Aug. 2008.

[30] M. Schönke, P. Feldens, D. Wilken, S. Papenmeier, C. Heinrich, J. S. von Deimling, P. Held, and S. Krastel, "Impact of *Lanice conchilega* on seafloor microtopography off the island of Sylt (German Bight, SE North Sea)," *Geo-Marine Letters*, vol. 37, p. 305–318, 2017.

[31] M. Schönke, L. Wiesenberg, I. Schulze, D. Wilken, A. Darr, S. Papenmeier, and P. Feldens, "Impact of sparse benthic life on seafloor roughness and high-frequency acoustic scatter," *Geosciences*, vol. 9, p. 454, Oct. 2019.

[32] M. Snellen, T. C. Gaida, L. Koop, E. Alevizos, and D. G. Simons, "Performance of multibeam echosounder backscatter-based classification for monitoring sediment distributions using multitemporal large-scale ocean data sets," *IEEE Journal of Oceanic Engineering*, vol. 44, pp. 142–155, Jan. 2019.